J. Appl. Numer. Optim. 7 (2025), No. 1, pp. 29-40
Available online at http://jano.biemdas.com
https://doi.org/10.23952/jano.7.2025.1.02

NUMERICAL RESOLUTION OF DIFFUSION EQUATIONS USING A WEAKLY MONOTONE FINITE VOLUME METHOD ON TETRAHEDRAL MESHES

MOHA ABERRAH[1], EL HOUSSAINE QUENJEL[2,*], PATRICK PERRÉ[2], MOHAMED RHOUDAF[1]

[1] *Faculty of Sciences, Moulay Ismaïl University, Meknès, Morocco*
[2] *Université Paris-Saclay, CentraleSupélec, Laboratoire de Génie des Procédés et Matériaux, Centre Européen de Biotechnologie et de Bioéconomie (CEBB), 3 rue des Rouges Terres, Pomacle, 51110, France*

Abstract. In this paper, we propose and extend the weakly monotone finite volume (WMFV) technique to discretize parabolic equations in 3D on tetrahedral meshes with anisotropy. The key idea is to introduce a nonlinear correction coefficient based on a centered approximation of the mobility function. This approach eliminates anti-diffusive fluxes, leading to a more accurate, robust, and efficient solver. Numerical validations are conducted to emphasize the accuracy and the stability of our method. Comparisons to the standard control volume finite element method and to its positive version are also provided.
Keywords. Anisotropy; Diffusion equations; Finite volumes; Parabolic equation; Tetrahedral meshes.
2020 Mathematics Subject Classification. 65M60, 65M12, 35K65.

1. INTRODUCTION

The field of variational numerical methods, such as finite elements, finite volumes or gradient schemes in general [11], is constantly evolving since the last decades. The purpose is to provide more accurate, robust, and efficient solutions to complex problems like diffusion processes. Elliptic terms are part of many mathematical and engineering problems. They are generally a preoccupation source of numerical instabilities when one deals with physical quantities [10]. Typical examples occur in heat transfer where the temperature must remain in certain physical ranges [2, 9]. A similar quest can be encountered in fluid flows in hygroscopic media where the saturation, density or concentration must obey physical bounds [7]. Standard schemes of type finite element or finite volumes do not allow to handle this issue with no complications. This can be translated by the works on the numerical stability subject referred as extremum-preserving and monotone schemes. There exist several nonlinear monotone methods in the literature to solve stationary diffusion problems or parabolic equations; see, e.g., [4, 5, 8, 16, 17, 18, 19, 22, 23] and the references therein. The practical implementation of these methods is challenging due to their complex and computationally expensive stencils. On the other hand, some positive approaches were studied in [6, 14, 21, 20]. They demonstrated their effectiveness in approximating complex flows in porous media or systems of chemotaxis [3, 15]. Their main idea is to utilize the degeneracy of the model or certain singular logarithmic functionals to

*Corresponding author.
E-mail address: el-houssaine.quenjel@centralesupelec.fr (E.H. Quenjel).
Received 20 April 2024; Accepted 21 September 2024; Published online 20 March 2025.

enforce positivity. However, the positive approach is not applicable if one intends to obtain a numerical solution that is greater than a tough initial condition including a ramp, for instance.

In our recent study [1], we developed and investigated a 2D weakly monotone finite volume (WMFV) discretization method to parabolic equations with anisotropy. Our main idea is to introduce a new nonlinear approximation of the nonlinear diffusion coefficient without changing the original stencil. 2D numerical tests were conducted to provide a good choice of the damping parameter so that one can ensure second order accuracy together with the weakly monotone property of the novel scheme.

In this paper, we propose, implement and validate a 3D extension to the WMFV scheme. Numerical results demonstrate that the method works well on unstructured simplices, providing nonpositive transmissibility coefficients, and deals with highly anisotropic tensors.

The rest of this work is structured as follows. In Section 2, we present the studied model. It is a pure diffusion problem with anisotropy and mixed boundary conditions. Section 3 recalls the discrete setting of the CVFE discretization as well as the associated notations. Section 4 exposes the 3D generalization of the WMFV method. We also prove the principle of the weak monotony preservation. The a priori estimates and the existence results are states where their proofs are direct adaptions from the 2D version. Section 5 shows the 3D numerical results. A particular accent is set on the accuracy, efficiency and the stability of the WMFV solver compared to the CVFE scheme and its positive version. Section 6 concludes and underlines some outlooks of the present paper.

2. Model Problem

The model problem is examined in the space-time domain $Q_{t_f} = \Omega \times \left(0, t_f\right)$, where Ω represents a bounded, open, and connected polygonal subset of $\mathbb{R}^d$ with $d = 3$. The real $t_f > 0$ accounts for the simulation final time. Let $\partial\Omega = \partial\Omega^D \cup \partial\Omega^N$, where the measure of $\partial\Omega^D$ is positive. The outward normal vector to $\partial\Omega^N$ is denoted by $\mathbf{n}$. The model equation is expressed in the following manner:

$$\phi u_t - \operatorname{div}(\eta(u)\Lambda\nabla u) = 0 \qquad \text{in } Q_{t_f}, \tag{2.1}$$

$$u(0,\cdot) = u^0 \qquad \text{in } \Omega, \tag{2.2}$$

$$u = 0 \qquad \text{on } \partial\Omega^D \times (0,t_f), \tag{2.3}$$

$$(\eta(u)\Lambda\nabla u)\cdot\mathbf{n} = 0 \qquad \text{on } \partial\Omega^N \times (0,t_f), \tag{2.4}$$

where the main unknown is u, $\phi(x) \in [\underline{\phi}, \overline{\phi}] \subset \mathbb{R}^+ \setminus \{0\}$ a.e. $x \in \Omega$ denotes the porosity, η is assumed to be continuous and nondecreasing function, Λ is a symmetric positive-definite diffusion tensor fulfilling $\Lambda\zeta\cdot\zeta/\|\zeta\|^2 \in [\underline{\Lambda}, \overline{\Lambda}] \subset \mathbb{R}^+ \setminus \{0\}$, for all $\zeta \neq 0$. The initial condition is an $L^2(\Omega)$-function such that $u^0 \geq g$ for a given function $x \to g(x) \geq 0 \in L^2(\Omega)$. Define Kirchhoff's transform $\xi(u) = \int_0^u \sqrt{\eta(s)}ds$.

For the definition and existence of a weak solution to problem (2.1)-(2.4), we refer to [14] and the references therein.

3. CVFE Discrete Setting

The CVFE-based methods make use of primal mesh and dual meshes. The primal mesh of Ω is a conforming partition $\mathscr{T}$ in the sense of finite elements. For each tetrahedral element

$K \in \mathscr{T}$, we denote by x_K its barycenter, h_K its diameter, and $|K|$ its Lebesgue measure. The set of vertices of $\mathscr{T}$ (resp. $K \in \mathscr{T}$) is denoted by $\mathscr{V}$ (resp. $\mathscr{V}_K$). The external vertices belonging to Dirichlet's boundary $\partial\Omega^D$ are given by the set $\mathscr{V}^D$. For each vertex $\mathbf{A} \in \mathscr{V}$, we define $\mathscr{K}_\mathbf{A}$ the set of elements sharing the vertex $\mathbf{A}$. Given $K \in \mathscr{K}_\mathbf{A}$, we define the set $\mathscr{F}_\mathbf{A}^K$ that accounts for the faces of K having in common the vertex $\mathbf{A}$. The vertices set of $\sigma \in \mathscr{F}_\mathbf{A}^K$ is referred to as $\mathscr{V}_\sigma$.

Let σ be in $\mathscr{F}_\mathbf{A}^K$ and $\mathbf{B} \in \mathscr{V}_\sigma \setminus \{\mathbf{A}\}$. We denote by $\sigma_{\mathbf{AB}}^{K,\star}$ the triangle generated by x_K, the center of sigma and the midpoint of the segment $e = [x_\mathbf{A}, x_\mathbf{B}]$, see Figure 1. Then, let $\omega_{\mathbf{A},\sigma_{\mathbf{AB}}^{K,\star}}$ stand for the cone with the apex $\mathbf{A}$ and the base $\sigma_{\mathbf{AB}}^{K,\star}$. As a result, one defines the dual volume $\omega_\mathbf{A}$ associated to $\mathbf{A}$ as

$$\omega_\mathbf{A} = \bigcup_{K \in \mathscr{K}_\mathbf{A}} \bigcup_{\sigma \in \mathscr{F}_\mathbf{A}^K} \bigcup_{\mathbf{B} \in \mathscr{V}_\sigma \setminus \{\mathbf{A}\}} \omega_{\mathbf{A},\sigma_{\mathbf{AB}}^{K,\star}}.$$

We designate by $\mathscr{F}_K^\star$ the dual faces $\sigma_{\mathbf{AB}}^{K,\star}$ included in the simplex K.

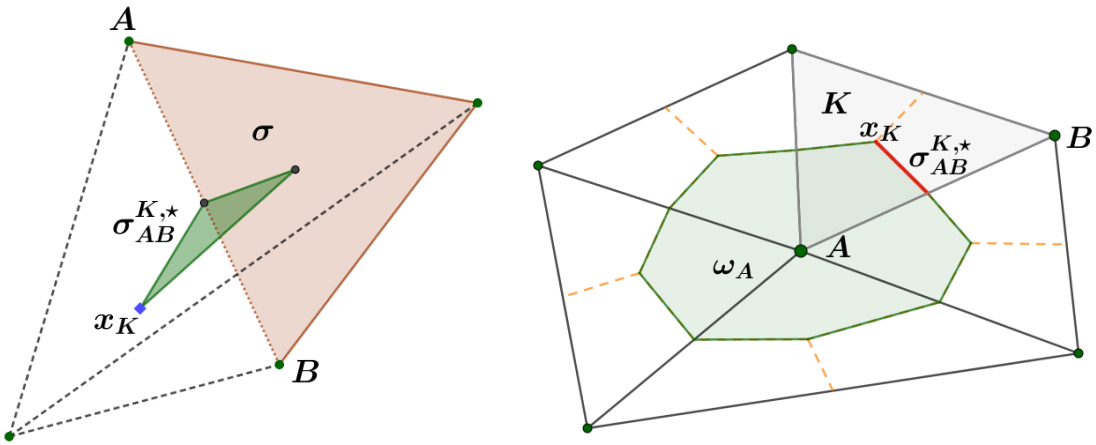

FIGURE 1. Dual interface $\sigma_{\mathbf{AB}}^{K,\star}$ separating the two control volumes $\omega_\mathbf{A}$ and $\omega_\mathbf{B}$ in the tetrahedral element K (left). 2D view of the whole volume $\omega_\mathbf{A}$ and surrounding neighbors.

Let ρ_K be the diameter of the largest ball included in the tetrahedral element K. The size as well as the regularity of $\mathscr{T}$ are respectively denoted by $h_\mathscr{T}$, $\theta_\mathscr{T}$. They are defined by

$$h_\mathscr{T} := \max_{K \in \mathscr{T}} (h_K), \quad \theta_\mathscr{T} := \max_{K \in \mathscr{T}} \frac{h_K}{\rho_K} > 0.$$

Assume that $\theta_{\mathscr{T}_h} \leqslant \Theta$ for a given refinement $\mathscr{T}_h$ of $\mathscr{T}$ [12]. Next, we define the following finite dimensional space:

$$\mathscr{H}_\mathscr{T} = \left\{ \Phi \in H^1(\Omega) \mid \Phi_{|K} \quad \text{is affine}, \quad \forall K \in \mathscr{T} \right\}.$$

The basis of $\mathscr{H}_\mathscr{T}$ is spanned by the shape functions $(\varphi_\mathbf{A})_{\mathbf{A} \in \mathscr{V}}$ such that $\varphi_\mathbf{A}(x_\mathbf{B}) = \delta_{\mathbf{AB}}$ for all $\mathbf{B} \in \mathscr{V}$, $\delta_{\mathbf{AB}}$ being the Kronecker symbol, for all $s_\mathscr{T} \in \mathscr{H}_\mathscr{T}$:

$$s_\mathscr{T} = \sum_{\mathbf{A} \in \mathscr{V}} s_\mathbf{A} \varphi_\mathbf{A}, \qquad \nabla s_\mathscr{T} = \sum_{\mathbf{A} \in \mathscr{V}} s_\mathbf{A} \nabla \varphi_\mathbf{A}.$$

The time discretization is given by the sequence $(t^n)_{n=0,\cdots,n_f}$ such that

$$t^0 = 0 < t^1 < \cdots < t^{n_f - 1} < t^{n_f} = t_f.$$

Without loss of generality, the time sub-intervals are uniform with a size δt.

Let us now introduce the transmissibility coefficient between $\mathbf{A}$ and $\mathbf{B}$

$$\Lambda_{\mathbf{AB}}^K = -\int_K \Lambda \nabla \varphi_{\mathbf{A}}(x) \cdot \nabla \varphi_{\mathbf{B}}(x) \mathrm{d}x = \Lambda_{\mathbf{BA}}^K \in \mathbb{R}. \tag{3.1}$$

We now state the discrete integration by parts, which is valuable for calculus. Its proof can be found in [6].

Lemma 3.1. *Let $s_{\mathscr{T}}$, $\psi_{\mathscr{T}} \in \mathscr{H}_{\mathscr{T}}$. Then*

$$\int_\Omega \Lambda \nabla s_{\mathscr{T}} \cdot \nabla \psi_{\mathscr{T}} \mathrm{d}x = \sum_{K \in \mathscr{T}} \sum_{\sigma_{\mathbf{AB}}^{K,\star} \in \mathscr{F}_K^\star} \Lambda_{\mathbf{AB}}^K (s_{\mathbf{A}} - s_{\mathbf{B}})(\psi_{\mathbf{A}} - \psi_{\mathbf{B}}). \tag{3.2}$$

4. Weakly Monotone Finite Volume Method

This section exposes the weakly monotone finite volume scheme and states some of its key theoretical properties.

4.1. Numerical scheme.

The weakly monotone finite volume scheme for the discretization of parabolic problem (2.1)-(2.4) is given by the following discrete system. The initial condition is approximated by

$$u_{\mathbf{A}}^0 = \frac{1}{|\omega_{\mathbf{A}}|} \int_{\omega_{\mathbf{A}}} u^0(x) \mathrm{d}x, \quad \forall \mathbf{A} \in \mathscr{V} \setminus \mathscr{V}^D, \quad u_{\mathbf{A}}^0 = 0, \quad \forall \mathbf{A} \in \mathscr{V}^D. \tag{4.1}$$

Then, at each time level $n \in \{0, \cdots, n_f - 1\}$, the balance equation writes

$$\phi_{\mathbf{A}}(u_{\mathbf{A}}^{n+1} - u_{\mathbf{A}}^n) + \frac{\delta t}{|\omega_{\mathbf{A}}|} \sum_{K \in \mathscr{K}_{\mathbf{A}}} \sum_{\mathbf{B} \in \mathscr{V}_K \setminus \{\mathbf{A}\}} V_{\mathbf{AB}}^{K,n+1} = 0, \quad \forall \mathbf{A} \in \mathscr{V} \setminus \mathscr{V}^D, \tag{4.2}$$

$$V_{\mathbf{AB}}^{K,n+1} = V_{\mathbf{AB}}^{K,n+1}(u_{\mathbf{A}}^{n+1}, u_{\mathbf{B}}^{n+1}) = \eta_{\mathbf{AB}}^{K,n+1} \Lambda_{\mathbf{AB}}^K (u_{\mathbf{A}}^{n+1} - u_{\mathbf{B}}^{n+1}), \tag{4.3}$$

$$u_{\mathbf{A}}^{n+1} = 0 \quad \forall \mathbf{A} \in \mathscr{V}^D. \tag{4.4}$$

The are many ways to define an approximation of $\eta_{\mathbf{AB}}^{K,n+1}$. Some of these expressions already have been discussed in [14], based on two crucial criteria: positivity and accuracy. As we mentioned before, we aim to maintain the weak monotonicity of the solution. The main idea is to consider a centered approximation of $\eta_{\mathbf{AB}}^{K,n+1}$ i.e.,

$$\eta_{\mathbf{AB}}^{K,n+1} = \eta_K^{n+1} \beta_{\mathbf{AB}}^{n+1}, \tag{4.5}$$

where

$$\eta_K^{n+1} = \frac{1}{\#\mathscr{V}_K} \sum_{\mathbf{A} \in \mathscr{V}_K} \eta\left(u_{\mathbf{A}}^{n+1}\right).$$

The novelty lies in the introduction of a specific nonlinear parameter $\beta_{\mathbf{AB}}^{n+1}$, where g is a given function defined in Section 2,

$$\beta_{\mathbf{AB}}^{n+1} = \begin{cases} 1 & \text{if } \Lambda_{\mathbf{AB}}^K \geq 0, \\ \beta(u_{\mathbf{A}}^{n+1} - g_{\mathbf{A}}) \beta(u_{\mathbf{B}}^{n+1} - g_{\mathbf{B}}), & \text{if } \Lambda_{\mathbf{AB}}^K < 0, \end{cases}$$

where

$$\beta(a) = 1 - \exp\left(\frac{-\max(a,0)^2}{2\gamma_{\mathscr{T}}^2}\right), \quad \forall a \in \mathbb{R}.$$

In this work, g depends on the studied problem and its choice is linked to the ranges of u_0 and the expected behavior of the numerical solution. Observe that β is nothing more than a regularization of the sign function. The choice of β is designed to preserve the flux conservation and reduce the amount of the added artificial viscosity thanks to the parameter $\gamma_{\mathscr{T}} > 0$. Its choice has been studied and chosen numerically in [1]. In terms of accuracy, an appropriate value for this parameter is $\gamma_{\mathscr{T}} = h_{\mathscr{T}}^2$.

4.2. **The weak monotonicity of the scheme.** Below, we present a brief description of positivity, the principle of minimal preservation, and the monotonicity in the context of the CVFE discretization of the studied transient model and the link between these notions to the weakly monotone property we claim in the paper. For all $A \in \mathscr{V}$ and $0 \leq n \leq n_f - 1$, the proposed scheme is said to be

- (i) positive if $u_A^0 \geq 0 \implies u_A^{n+1} \geq 0$, [14, 20];
- (ii) minimum-preserving if $u_A^0 \geq a \implies u_A^{n+1} \geq a$ for some scalar $a > 0$;
- (iii) weakly monotone if $u_A^0 \geq g_A \implies u_A^{n+1} \geq g_A$, some function $g \geq 0$;
- (iv) monotone if the flux $V_{\mathbf{AB}}^{K,n+1}\left(u_{\mathbf{A}}^{n+1}, u_{\mathbf{B}}^{n+1}\right)$ is nondecreasing with respect to the first argument and nonincreasing with respect to the second argument [16].

It can be easily checked that

$$(iv) \implies (iii) \implies (ii) \implies (i).$$

Note that the nonlinear CVFE scheme (4.1)-(4.4) is monotone (fulfills property (iv)) if all the transmissibility coefficients $\Lambda_{\mathbf{AB}}^K \geq 0$. However, this condition does not hold true on generic tetrahedral elements and anisotropic tensors. Our goal is to alleviate this condition by introducing the concept of the weak monotonicity.

Let us state and prove the main stability result of this work.

Proposition 4.1. *The finite volume scheme* (4.1)-(4.4) *is weakly monotone, i.e.,* $u_{\mathbf{A}}^n \geq g_{\mathbf{A}}$ *for all* $n \in \left[0, n_f\right]$ *and for all* $\mathbf{A} \in \mathscr{V}$.

Proof. We use both induction on n and the proof by contradiction. Consider $\omega_{\mathbf{A}}$ such that $u_{\mathbf{A}}^{n+1} = min_{\mathbf{B} \in \mathscr{V} \setminus \mathscr{V}_D} u_{\mathbf{B}}^{n+1} < g_{\mathbf{A}}$. We multiply the equation (4.2) corresponding to $\mathbf{A}$, by $(u_{\mathbf{A}}^{n+1} - g_{\mathbf{A}})$.

$$(u_{\mathbf{A}}^{n+1} - u_{\mathbf{A}}^n)(u_{\mathbf{A}}^{n+1} - g_{\mathbf{A}}) + \frac{\delta t}{|\omega_{\mathbf{A}}|} \sum_{K \in \mathscr{K}_{\mathbf{A}}} \sum_{\mathbf{B} \in \mathscr{V}_K \setminus \{\mathbf{A}\}} \Lambda_{\mathbf{AB}}^K (u_{\mathbf{A}}^{n+1} - u_{\mathbf{B}}^{n+1})(u_{\mathbf{A}}^{n+1} - g_{\mathbf{A}}) = 0.$$

Use the fact that $\Lambda_{\mathbf{AB}}^K = \left(\Lambda_{\mathbf{AB}}^K\right)^+ + \left(\Lambda_{\mathbf{AB}}^K\right)^-$ to write

$$\begin{aligned}(u_{\mathbf{A}}^{n+1} - u_{\mathbf{A}}^n)(u_{\mathbf{A}}^{n+1} - g_{\mathbf{A}}) + \frac{\delta t}{|\omega_{\mathbf{A}}|} \sum_{K \in \mathscr{K}_{\mathbf{A}}} \sum_{\mathbf{B} \in \mathscr{V}_K \setminus \{\mathbf{A}\}} \left(\Lambda_{\mathbf{AB}}^K\right)^+ (u_{\mathbf{A}}^{n+1} - u_{\mathbf{B}}^{n+1})(u_{\mathbf{A}}^{n+1} - g_{\mathbf{A}}) \\ + \frac{\delta t}{|\omega_{\mathbf{A}}|} \sum_{K \in \mathscr{K}_{\mathbf{A}}} \sum_{\mathbf{B} \in \mathscr{V}_K \setminus \{\mathbf{A}\}} \left(\Lambda_{\mathbf{AB}}^K\right)^- \beta_{\mathbf{AB}}^{n+1} (u_{\mathbf{A}}^{n+1} - u_{\mathbf{B}}^{n+1})(u_{\mathbf{A}}^{n+1} - g_{\mathbf{A}}) = 0.\end{aligned}$$

Because of $(u_{\mathbf{A}}^{n+1} - g_{\mathbf{A}}) < 0$, $\beta_{\mathbf{AB}}^{n+1} = 0$. Therefore, the last summation term vanishes.

Next, splitting the accumulation term, we have

$$(u_{\mathbf{A}}^{n+1}-g_{\mathbf{A}})^2-(u_{\mathbf{A}}^{n}-g_{\mathbf{A}})(u_{\mathbf{A}}^{n+1}-g_{\mathbf{A}})$$
$$+\frac{\delta t}{|\omega_{\mathbf{A}}|}\sum_{K\in\mathscr{K}_{\mathbf{A}}}\sum_{\mathbf{B}\in\mathscr{V}_K\setminus\{\mathbf{A}\}}\left(\Lambda_{\mathbf{AB}}^K\right)^+(u_{\mathbf{A}}^{n+1}-u_{\mathbf{B}}^{n+1})(u_{\mathbf{A}}^{n+1}-g_{\mathbf{A}})=0. \tag{4.6}$$

All the terms of (4.6) are nonnegative. Particularly, one infers that $(u_{\mathbf{A}}^{n+1}-g_{\mathbf{A}})^2=0$, which implies that $u_{\mathbf{A}}^{n+1}=g_{\mathbf{A}}$. This contradicts the posed hypothesis. Consequently, the monotony of the scheme does not allow $u_{\mathbf{A}}^{n+1}$ to be lower than $g_{\mathbf{A}}$. Hence, we deduce

$$u_{\mathbf{A}}^{n+1}=min_{\mathbf{B}\in\mathscr{V}\setminus\mathscr{V}_D}u_{\mathbf{B}}^{n+1}\geqslant g_{\mathbf{A}},$$

as required. □

4.3. **A priori estimates and existence result.** All the properties in the sequel were proved in [1] in 2D. The 3D proofs are similar.

Lemma 4.1. *There exists a constant C that depends only on $\theta_{\mathscr{T}}$, $\underline{\Lambda}$ and $\bar{\Lambda}$ such that, for any $u_{\mathscr{T}}\in\mathscr{H}_{\mathscr{T}}$,*

$$\sum_{K\in\mathscr{T}}\sum_{\sigma_{\mathbf{AB}}^{K,\star}\in\mathscr{F}_K^\star}|\Lambda_{\mathbf{AB}}^K|(u_{\mathbf{A}}-u_{\mathbf{B}})^2\leqslant C\sum_{K\in\mathscr{T}}\sum_{\sigma_{\mathbf{AB}}^{K,\star}\in\mathscr{F}_K^\star}\Lambda_{\mathbf{AB}}^K(u_{\mathbf{A}}-u_{\mathbf{B}})^2=C\int_\Omega\Lambda\nabla u_{\mathscr{T}}\cdot\nabla u_{\mathscr{T}}\mathrm{d}x.$$

Proposition 4.2. *Let $(u_{\mathbf{A}}^{n+1})_{\mathbf{A}\in\mathscr{V},n=0,\cdots,n_f-1}$ be a solution to system (4.1)-(4.4). Then there exists $C>0$ depending only on the physical data and $\theta_{\mathscr{T}}$ such that*

$$\sum_{n=0}^{n_f-1}\delta t\left\|\nabla\xi_{\mathscr{T}}^{n+1}\right\|_{L^2(\Omega)^2}^2\leqslant C, \tag{4.7}$$

$$\sum_{n=0}^{n_f-1}\delta t\sum_{K\in\mathscr{T}}\sum_{\sigma_{\mathbf{AB}}^{K,\star}\in\mathscr{F}_K^\star}|\Lambda_{\mathbf{AB}}^K|\eta_{\mathbf{AB}}^{K,n+1}\left(u_{\mathbf{A}}^{n+1}-u_{\mathbf{B}}^{n+1}\right)^2\leqslant C. \tag{4.8}$$

Proposition 4.3. *There exists a solution $(u_{\mathbf{A}}^{n+1})_{\mathbf{A}\in\mathscr{V},n=0,\cdots,n_f-1}$ to the weakly monotone finite volume scheme (4.1)-(4.4). It further satisfies the physical range claimed in Proposition 4.1.*

5. Numerical Experiments

This section presents some numerical tests aiming to validate the 3D WMFV approach and its capability to excellently preserve the prescribed bounds. Comparisons to the conventional CVFE approach are also provided.

The domain of interest is the cube $\Omega=[0,1]^3$. It is discretized with a sequence of tetrahedral elements that are taken from the $3D$ benchmark on anisotropic diffusion problems [13]. The first element and the second one of this mesh family are depicted in Figure 2. Table 1 reports size, number of vertices, and cells for each mesh. The final time is fixed to $t_f=0.2$, and the porosity function is $\phi=1$. The resulting scheme is formulated in a nonlinear algebraic system. It is solved by using Newton's method with a given tolerance 10^{-6}, and a stopping criterion based on the ℓ^2-norm of the residual. Because of the first order implicit Euler scheme that is considered in time, the time stepping is $\delta t=0.1h_{\mathscr{T}}{}^2$.

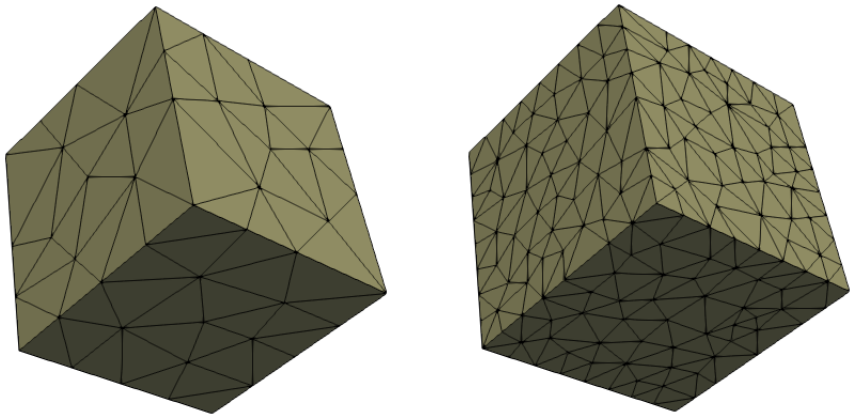

FIGURE 2. First and second element of the used tetrahedral meshes.

$h_{\mathscr{T}}$	0.250	0.125	0.063	0.031
Nbr of vertices	80	488	857	1601
Nbr cells	215	2003	3898	7711

TABLE 1. Size, number of vertices and number of cells of the used tetrahedral meshes.

5.1. **Example 1: Accuracy and positivity test.** The first aim here is to study the accuracy and the efficiency of the WMFV scheme compared to the CVFE approach. The second is to ensure that the WMFV scheme is also positive in the framework of this test.

For this purpose, we consider the anisotropic heat equation. Then, the mobility function is constant, i.e., $\eta(u) = 1$. The equation is supplemented by the homogeneous Neumann condition on the full boundary

$$u_t - \mathrm{div}(\Lambda \nabla u) = 0, \qquad \text{where} \qquad \Lambda = \begin{pmatrix} a_x & 0 & 0 \\ 0 & a_y & 0 \\ 0 & 0 & a_z \end{pmatrix}.$$

The tensor Λ is taken highly anisotropic with $a_x = a_y = 1$ and $a_z = 100$. The function g is fixed to zero because we are interested in the positivity quest. An exact solution to the above problem can be manufactured under the form: for $(x,y,z) \in \Omega$, $t \in (0,t_f)$

$$u(x,y,z,t) = \frac{1}{2}\Big(1 + \cos(\pi x)\cos(\pi y)\exp(-2\pi^2 t)\Big).$$

The linear CVFE scheme is solved by using Matlab's linear solver. The results are presented in Table 2. The accuracy (measured in $L^2(Q_{t_f})$-norm) as well as the convergence rates are quite similar. The CPUt refers to the CPU time (in seconds) that quantifies the computational cost of the resolution algorithm. It is bigger for the WMFV method as the mesh is refined. This is because of the Newton iterations implemented to solve the nonlinear algebraic system, see Table 3. They are increasing as $h_{\mathscr{T}}$ is decreasing. In addition, observe that the CVFE scheme suffers from oscillations generated by anisotropy, unlike the nonlinear WMFV scheme which preserves the positivity of the solution. This behavior can be viewed directly on the 3D plot exhibited in Figure 3 of the computed solutions. The magenta dots highlight the location of negative values. The solution of WMFV methodology is free of these oscillations and maintains its positivity.

	CVFE				WMFV			
$h_{\mathscr{T}}$	L^2-errors	Rate2	u_{min}	CPUt	L^2-errors	Rate2	u_{min}	CPUt
0.250	0.1030	-	0	0.10	0.1057	-	0	0.19
0.125	0.0516	1.1474	-0.0082	3.15	0.0519	1.1810	0	3.97
0.063	0.0351	2.0463	-0.0085	10.37	0.0353	2.0572	0	11.49
0.031	0.0224	2.1588	-0.0040	42.79	0.0224	2.1698	0	51.39

TABLE 2. Accuracy results of the CVFE and WMFV schemes.

$h_{\mathscr{T}}$	0.250	0.125	0.063	0.031
Nbr Newton	147	608	847	1511

TABLE 3. Accumulated number of Newton iterations for the WMFV scheme.

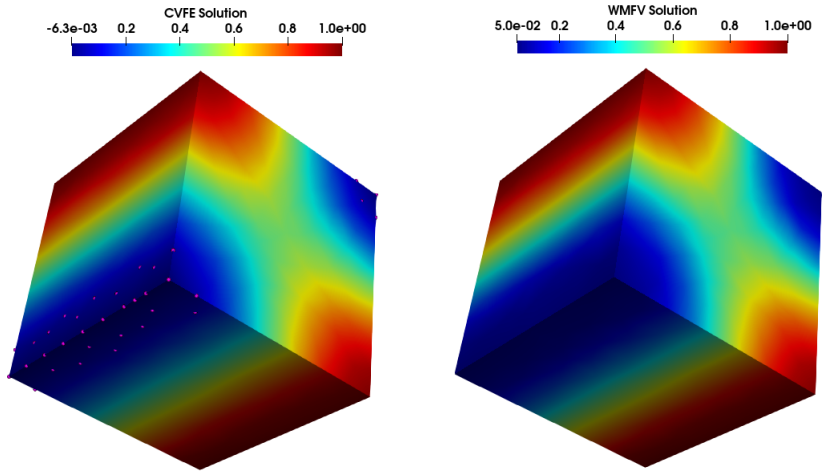

FIGURE 3. Numerical solution of the CVFE (resp. WMFV) scheme on the left (resp. right) at $t = 0.2$. The dots indicate the location of undershoots.

5.2. **Example 2: Weak monotony preservation.** The aim of this example is to test the weak monotonicity preservation in the case of anisotropic nonlinear equation with a piecewise linear initial condition. We also stress that positive schemes are unable to capture all the stability features of the numerical solution.

The studied model is:

$$u_t - \operatorname{div}(\eta(u)\Lambda\nabla u) = 0,$$

where the mobility function is $\eta(u) = 2u/(1+u^2)$. The chosen tensor is anisotropic, heterogeneous, and rotating. It is deduced from the matrix product

$$\Lambda = \begin{pmatrix} \cos(\pi x) & -\sin(\pi x) & 0 \\ \sin(\pi x) & \cos(\pi x) & 0 \\ 0 & 0 & 1 \end{pmatrix} \begin{pmatrix} 1 & 0 & 0 \\ 0 & 100 & 0 \\ 0 & 0 & 1 \end{pmatrix} \begin{pmatrix} \cos(\pi x) & \sin(\pi x) & 0 \\ -\sin(\pi x) & \cos(\pi x) & 0 \\ 0 & 0 & 1 \end{pmatrix}.$$

The initial condition is taken as

$$u(x,y,z,0) = \begin{cases} -\frac{1}{0.3}x+1 & \text{if} \quad 0 \le x \le 0.3, \\ 0 & \text{if} \quad 0.3 < x \le 0.7, \\ \frac{1}{(1-0.7)}(x-0.7) & \text{if} \quad 0.7 < x \le 1. \end{cases} \tag{5.1}$$

Observe that the initial solution degenerates on $[0.3,0.7]\times[0,1]\times[0,1]$. The problem is closed with the boundary conditions:

- $\partial\Omega^D = \{x=0\}\cup\{x=1\}$ Dirichlet's condition agrees with u_0 given in (5.1).
- $\partial\Omega^N = \{y=0\}\cup\{y=1\}\cup\{z=0\}\cup\{z=1\}$ homogeneous Neumann's boundary condition is maintained.

Here g is fixed to u_0, because the expected solution will remain in the convex hall generated by the bounds of u_0. Such behavior of the solution is widespread in heat transfer within materials or in fluid flows in porous media.

Three numerical schemes are implemented. The standard CVFE scheme, the accurate positive CVFE approach developed in [14], and the proposed WMFV method of the current work. The point is to look at the stability feature of each discretization strategy.

The outcomes of this test are given in Figure 4. The first column shows the approximate solution on the orthotropic slices of the domain, at $t = 0.0014$. The third mesh is considered here. The magenta dots account for the location where the numerical solution is strictly less than u_0. The second column shows 1D plot of the solution across the line connecting the points $(0,1,0.29)$ and $(1,1,0.29)$. Three times are considered $t \in \{0, 0.0014, 0.0109\}$.

The CVFE solution is very sensitive to sever anisotropy. The corresponding solver produces a lot of undershoots at the first iterations in time. The 1D plot shows the overflow of the solution on the bounds of the initial datum. Furthermore, negatives values are recorded. This is standard in the literature of finite elements/ finite volumes with no corrections in the presence of strong anisotropy.

The positive scheme of [14] only captures the positive part of the computed solution and ignores the overflow problem. By its construction, the scheme is incapable to detect whether the solution is less than the function g or not.

However, the WMFV strategy enjoys excellent stability features, and yields to a good behavior that captures all the information about the evolution of the expected solution. Additionally, The Newton solver begins with 10 iterations at the first time steps and downs to 3 iterations afterwards. The solution remains in its ranges as claimed in Lemma 4.1.

To sum up, the WMFV scheme provides solutions that respect the applicable physical limits. Additionally, it offers a precision similar to that of the CVFE version and is capable of generating the expected numerical solution regardless the selected initial data or imposed diffusion tensor. Let us refer to [1] for more test cases and comparisons in 2D.

6. Conclusion

In this paper, we proposed a 3D numerical extension to the weakly monotone finite volume method that we recently developed. It was applied in the case of linear and nonlinear pure diffusion equation on tetrahedral meshes with anisotropy. Our main idea is to eliminate the anti-diffusive contributions thanks to a nonlinear correction that is included in the fluxes. It takes into account the ranges of the initial data whenever the solution is increasing in time.

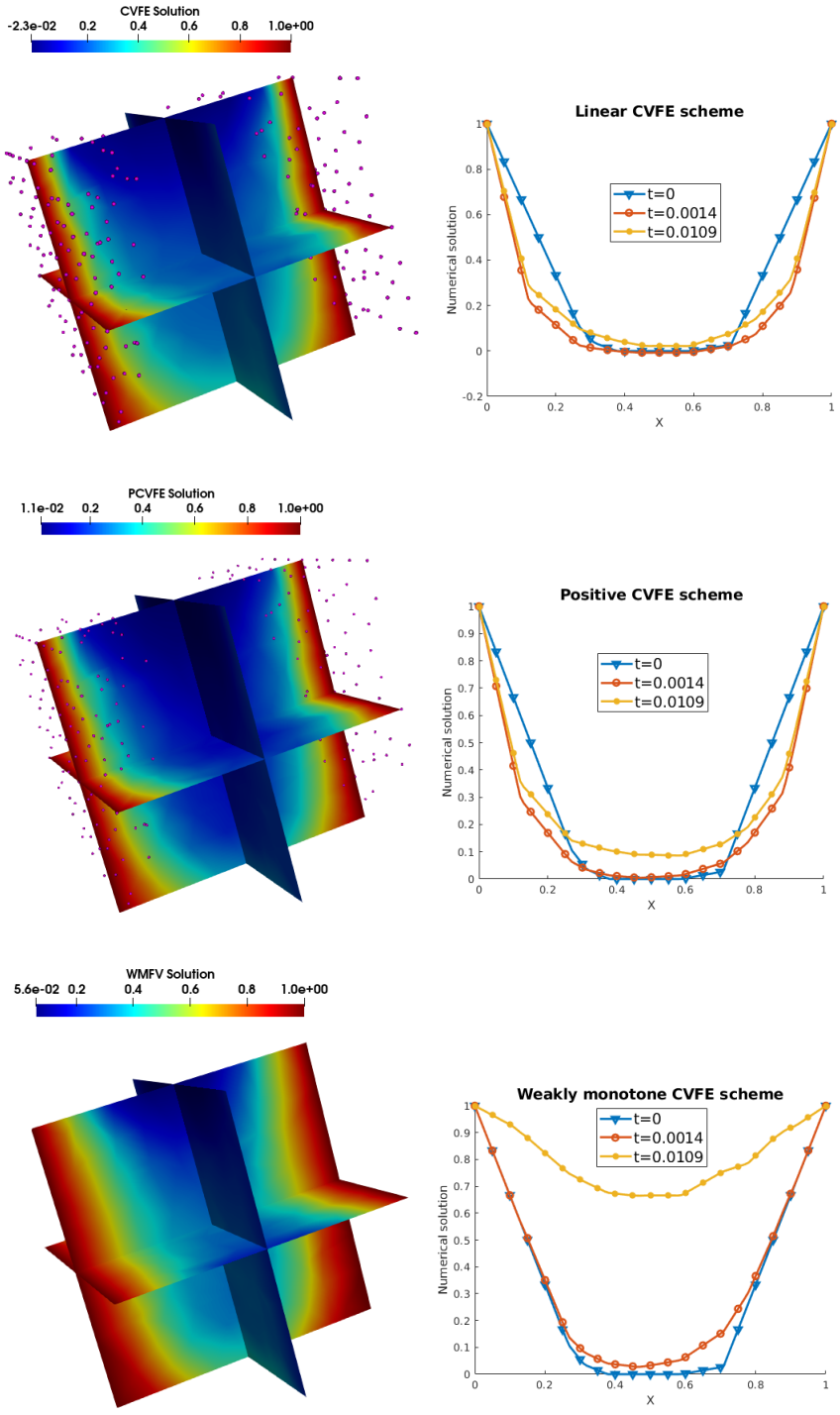

FIGURE 4. Behavior of the solution on the standard slices of the domain Ω for the CVFE, positive CVFE and WMFV schemes at $t = 0.0014$ (left). The dots refers to the location of undershoots. 1D plot of the solution (right).

We gave the proof of the proposed weak monotonicity. The a prior estimates fulfilled by the WMFV scheme were also presented. They follow the same steps as in the 2D setting. Two numerical examples were examined. The first one aims to ensure that the WFMV is accurate of second order in space. The second one highlights the monotony preservation in the case of piecewise linear initial solution and in the presence of highly anisotropic heterogeneous diffusion tensor. The outcomes are compared to the standard CVFE and the positive CVFE methods. Good results are in favor of the WMFV strategy. In the future, We are interested in testing the robustness and the efficiency the WMFV methodology for coupled systems. And we are going to add a nonlinear convection term and couple the resulting equation to Darcy flows in highly anisotropic hygroscopic media.

Acknowledgments
Communauté urbaine du Grand Reims, Département de la Marne, Région Grand Est and European Union (FEDER Champagne-Ardenne 2014-2020) are acknowledged for their financial support to the Chair of Biotechnology of CentraleSupélec and the Centre Européen de Biotechnologie et de Bioéconomie (CEBB).

REFERENCES

[1] M. Aberrah, E.H. Quenjel, P. Perré, M. Rhoudaf, Weakly monotone finite volume scheme for parabolic equations in strongly anisotropic media, J. Appl. Math. Comput. 69 (2023), 3289–3316.
[2] T.L. Bergman, A.S. Lavine, F.P. Incropera, D.P. Dewitt, David P. DeWitt, Fundamentals of Heat and Mass Transfer, John Wiley & Sons, 2011.
[3] K. Brenner, R. Masson, E.H. Quenjel, Vertex approximate gradient discretization preserving positivity for two-phase Darcy flows in heterogeneous porous media, J. Comput. Phys. 409 (2020), 109357.
[4] E. Burman, A. Ern, Discrete maximum principle for Galerkin approximations of the Laplace operator on arbitrary meshes, Comptes Rendus Math. 338 (2004), 641-646.
[5] C. Cancès, M. Cathala, C.L. Potier, Monotone corrections for generic cell-centered finite volume approximations of anisotropic diffusion equations, Numer. Math. 125 (2013),387-417.
[6] C. Cancès, C. Guichard, Convergence of a nonlinear entropy diminishing control volume finite element scheme for solving anisotropic degenerate parabolic equations, Math. Comput. 85 (2016), 549-580.
[7] G. Chavent, J. Jaffré, Mathematical models and finite elements for reservoir simulation: single phase, multiphase and multicomponent flows through porous media, Elsevier, 1986.
[8] N. Dahmen, J. Droniou, F. Rogier, A cost-effective nonlinear extremum-preserving finite volume scheme for highly anisotropic diffusion on Cartesian grids, with application to radiation belt dynamics, J. Comput. Physics 463 (2022), 111258.
[9] A.K. Datta, Porous media approaches to studying simultaneous heat and mass transfer in food processes. I: Problem formulations, J. Food Engineering 80 (2007), 80-95.
[10] J. Droniou, Finite volume schemes for diffusion equations: Introduction to and review of modern methods, Math. Model. Methd. Appl. Sci. 24 (2014), 1575-1619.
[11] J. Droniou, R. Eymard, T. Gallouët, C. Guichard, R. Herbin, The Gradient Discretisation Method, vol. 82, Springer, 2018.
[12] A. Ern, J.L. Guermond, Theory and practice of finite elements, vol. 159, Springer Science & Business Media, 2013.
[13] R. Eymard, G. Henry, R. Herbin, F. Hubert, R. Klöfkorn, G. Manzini, 3D benchmark on discretization schemes for anisotropic diffusion problems on general grids, Finite Volumes for Complex Applications VI Problems & Perspectives, pp. 895–930, Springer, 2011. DOI: 10.1007/978-3-642-20671-9_89
[14] C. Guichard, E.H. Quenjel, Weighted positive nonlinear finite volume method for dominated anisotropic diffusive equations, Adv. Comput. Math. 48 (2022), 1-63.

[15] M. Ibrahim, E.H. Quenjel, M. Saad, Positive nonlinear DDFV scheme for a degenerate parabolic system describing chemotaxis, Comput. Math. Appl. 80 (2020), 2972-3003.
[16] I.V. Kapyrin, A family of monotone methods for the numerical solution of three-dimensional diffusion problems on unstructured tetrahedral meshes, Doklady Math. 7 (2007), 734-738.
[17] C.L. Potier, Correction non linéaire d'ordre 2 et principe du maximum pour la discrétisation d'opérateurs de diffusion, Comptes Rendus Math. 352 (2014), 947-952.
[18] K. Lipnikov, D. Svyatskiy, Y. Vassilevski, A monotone finite volume method for advection–diffusion equations on unstructured polygonal meshes, J. Comput. Physics 229 (2010), 4017-4032.
[19] K. Lipnikov, D. Svyatskiy, Y. Vassilevski, Interpolation-free monotone finite volume method for diffusion equations on polygonal meshes, J. Comput. Physics 228 (2009), 703-716.
[20] E.H. Quenjel, Enhanced positive vertex-centered finite volume scheme for anisotropic convection-diffusion equations, ESAIM: Math. Model. Numer. Anal. 54 (2020), 591-618.
[21] E.H. Quenjel, M. Saad, M. Ghilani, M.B. Chatard, Convergence of a positive nonlinear DDFV scheme for degenerate parabolic equations, Calcolo 57 (2020), 1-38.
[22] Z. Sheng, G. Yuan, The finite volume scheme preserving extremum principle for diffusion equations on polygonal meshes, J. Comput. Physics 230 (2011), 2588-2604.
[23] G. Yuan, Z. Sheng, Monotone finite volume schemes for diffusion equations on polygonal meshes, J. Comput. Physics 227 (2008), 6288-6312.